A Method for Producing Single Crystal Foils of Tin from the Melt

Masashige KOYAMA, Yoshikazu TSUJII and Shigeo MAEDA*

(Takaki Laboratory)

Received March 30, 1964

A Method for producing thin single crystals of white tin has been devised by means of the Bridgman method, using a special type of glass mould, in order to investigate the relationship between the thickness of specimens and the formation of the striation-type substructure, that is, the dislocation density. It is possible to produce the single crystal foils of about 0.01 cm in thickness by this technique.

Furthermore, the relation of growth conditions with substructures has been examined by X-ray methods, and it has been found that the striation-type subboundaries are formed even in the specimens grown on such a condition that the striation-type substructure should not be formed under a consideration based on Frank's theory.

I. INTRODUCTION

In metal single crystals grown from the melt, two kinds of substructures have generally been observed[1]: one is the impurity substructure, named "corrugation" by Rutter and Chalmers[2], whose generation is attributed to the solute-impurities included in metals; the other is the misoriented substructure, named "striation" by Teghtsoonian and Chalmers[3], subboundaries of which consist of the arrangement of edge-dislocations. The former is formed parallel to the direction of heat flow and is suppressed under such a condition as high purity, high temperature gradient and low rate of growth. On the other hand, an explanation of the latter had primarily been postulated by Teghtsoonian et al.[3] on a vacancy mechanism. Lately, Frank[4] developed a more detailed picture of the mechanism of collapsing vacancy discs in order to explain the origin, size and initial misorientation of the substructure of the striation-type qualitatively. Recently, this mechanism of dislocation-loop-formation based upon the vacancy condensation, has been examined in a quantitative manner by Schoeck and Tiller[5], Elbaum[6], Jackson[7]: Schoeck et al. have shown that the above mentioned mechanism by Frank may be inapplicable, because both the number of dislocation loops formed by the collapsing of vacancy discs and the climb rate of dislocations are insufficient for the formation of the striation-type subboundaries; Elbaum has examined the formation of dislocations by the collapsing vacancy disc mechanism for aluminium, copper, silicon and germanium, and has shown that this mechanism is important in the case of metals but the loop may not reach a size detectable by means of the optical

* 小山　昌重，辻井　芳一，前田　繁男

microscope in silicon and germanium; furthermore, Jackson has concluded that none of the various mechanisms suggested for the formation of dislocations can perfectly explain the dislocations found in melt-grown crystals. Thus, there has not yet been known any sufficient mechanism to account for the formation of the striation-type substructure.

Elbaum[8] has examined the relationship between the dimensions of specimens and the dislocation densities with regard to aluminium single crystals in the shape of carrot by Lang's X-ray Method[9], and further has shown that no dislocation is observed in the fine part below 0.5 mm in diameter in the super-pure specimen grown under a very carefully controlled condition[10].

In order to investigate the relationship between the thickness of specimens and the formation of the striation-type substructure, that is, the dislocation density, the authors have devised a method for producing the single crystal foils of white tin from the melt by means of Bridgman method. The specimens thus prepared have been examined by X-ray diffraction methods.

II. EXPERIMENTAL

i) Preparation of Glass Mould

Two sheets of glass (1×5×0.14 cm in dimensions) were cut down from the photographic plate and two thin sheets of glass (0.3×5×t cm in dimensions) were also prepared. Then the latter was so sandwiched in between the former that the longer edges of both sheets were put together, and were sealed with

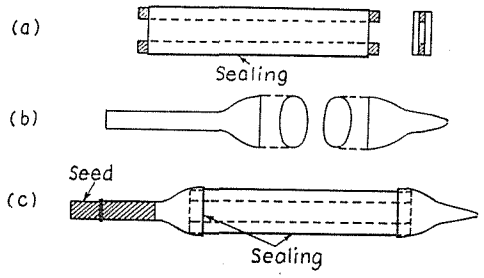

Fig. 1. Preparation of glass mould.

alumina slip mixed with sodium silicate as shown in Fig. 1(a). After each of two glass tubes shown in Fig. 1(b) was put on the shorter edges of the above mentioned set of glass sheets, the glass mould thus assembled was sealed as shown in Fig. 1(c) and was desiccated in a drier.

ii) Conditions

The purity of white tin used, the thickness of speciments, t, the rate of growth, R, and the temperature gradient of the electric furnace are given in Table 1.

iii) Procedure

After sucking the molten tin in the pre-heated glass mould from one end

Table 1. Experimental conditions.

Purity	Thickness (t)	Lowering Speed (R)$\left(\frac{\text{mm/min}}{\text{(cm/sec)}}\right)$	(Temp. Grad. (G)=25°/cm)
99.8%	0.015 cm	6.1–6.7 (1.1×10⁻²) 1.7–1.8 (2.8×10⁻³)	0.1–0.11 (1.7×10⁻⁴) 0.09–0.11 (1.5×10⁻⁴) 0.08–0.11 (1.3×10⁻⁴)
	0.142 cm	13–16 (2.4×10⁻²) 6–7 (1.1×10⁻²) 1 (1.7×10⁻³) 0.2–0.3 (4.2×10⁻⁴)	

in air, a single crystal seed of a desired crystallographic orientation was welded to the other end of the charge as shown in Fig. 1(c), and the crystal was grown in air by the Bridgman method. The crystallographic arrangement

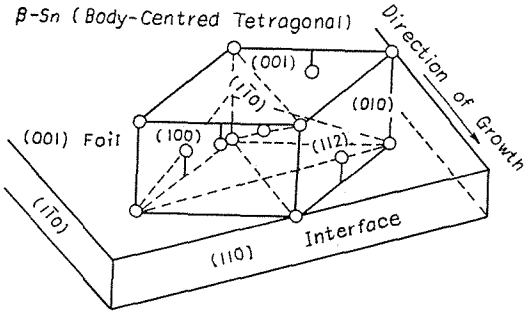

Fig. 2. Crystallographic arrangement.

in this case is illustrated in Fig. 2. After solidification, both flat sides of the mould were covered with paraffin and the mould thus prepared was sunk into fluoric acid solution in order to remove both the glass tubes and one of the flat glass plates. In this case, if the inside of the removed glass plate had faintly been covered with silicon oil previously, its removal could be accomplished more easily. The specimen surfaces thus exposed were examined with X-rays. Berg-Barrett's method* was applied to both finding out of substructures and measuring of those widths. On the other hand, Kato's method** was used in measuring of the misorientation of substructures. In each case, (112) reflections of Cu$K\alpha$ radiation from the surfaces of specimens were mainly observed.

III. EXPERIMENTAL RESULTS

i) Production of Single Crystal Foils

The unetched macro-structures of the specimens of 0.015 and 0.142 cm in thickness are shown in Figs. 3(a) and (b) respectively, where the lowering speeds, R, are about 2.8×10^{-3} and 1.1×10^{-2} cm/sec respectively. The direction of growth ([110]-direction of easy growth) is designated with an arrow. Many

* So-called "X-ray diffraction microscopy"[11].

** An X-ray diffraction technique using a bent-quartz monochromater of the transmission type[12].

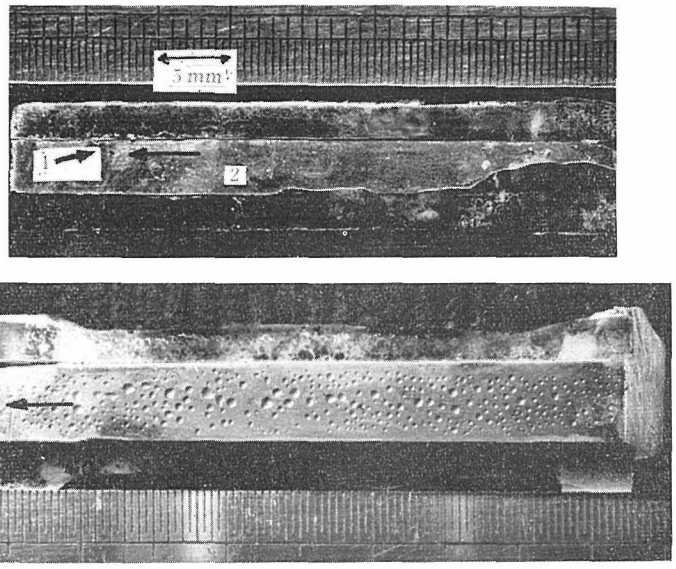

Fig. 3. The unetched macro-structures of the specimens grown at $R \simeq 2.8\times10^{-3}$ cm/sec ($t=0.015$ cm) in (a) and at $R \simeq 1.1\times10^{-2}$ cm/sec ($t=0.142$ cm) in (b) respectively.

small hollows observed in Fig. 3(b) seem to be formed not only at the freezing process of the molten charge sucked in, but also during the crystal growth. When the silicon oil covered is too much, the formation of hollows seems to become violent. Some holes penetrating the specimen through both flat surfaces, are formed only in the specimens of 0.015 cm in thickness. The undesirable defects mentioned above may be avoided by charging in vacunm.

It seems that the single crystal foils of tin can be produced to the extent of 0.01 cm in thickness by this technique.

ii) Specimens of 0.01 cm in Thickness

The spacing of the impurity substructure increases with the decrease of the rate of growth as known in general. For example, a set of two pieces of Berg-Barrett Photographs and an optical microscope structure with regard to the specimen shown in Fig. 3(a), are shown in Figs. 4(a) and (b) respectively; here the longer arrows designate the direction of growth. The lines running along the specimen axis represent the impurity subboundaries. Fig. 5* shows a (112) reflection of CuKα doublet from a part of the aforesaid specimen using the bent-quartz-monochromater-technique. Each of the reflection spots corresponds to that from each of the neighbouring impurity substructure. The values of the misorientation between each of the neighbouring corrugations expressed in numerals are given in the table beside the photograph, where $\Delta\theta_h$ and $\Delta\theta_v$ represent the misorientation angles around the horizontal and vertical axes respectively; here the positive or negative sign represents the

* The inclination of the reflection lines is attributed to the deviation of the secimen surface from (001) plane.

(a)

(b)

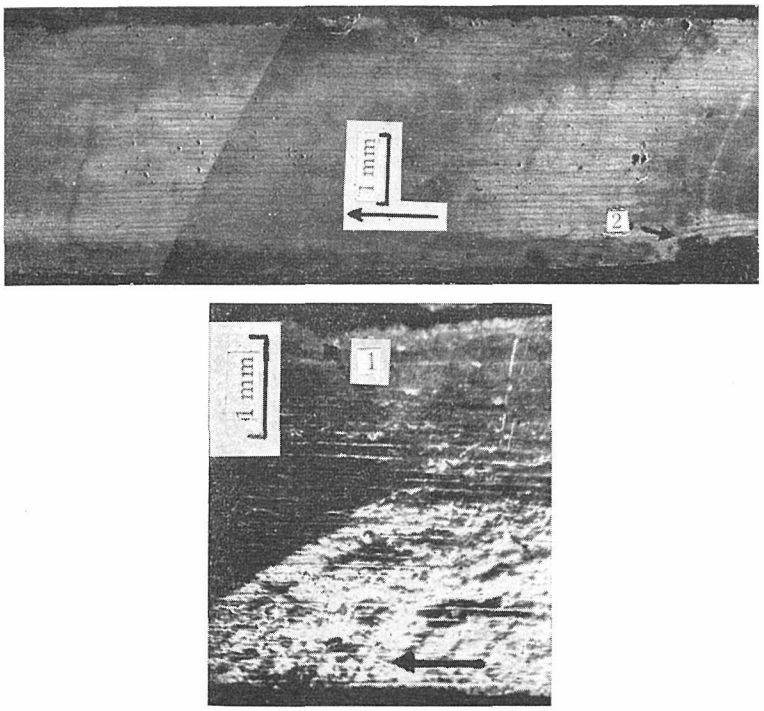

Fig. 4. (a) A set of two pieces of Berg-Barrett photographs reflected from the surface of the specimen shown in Fig. 3 (a). The longer arrow designates the direction of growth.
(b) An optical microscope structure obtained from the specimen surface shown in Fig. 3 (a).
The shorter arrows 1 and 2 in Fig. 3 (a) correspond to those in this figure.

	$\Delta\theta_h$	$\Delta\theta_v$
1—2	+1.8′	− 1′
2—3	+2.4′	−0.1′
3—4	+1.7′	+1.1′
4—5	+2.0′	
5—6	+0.8′	
6—7	+1.3′	+1.3′
7—8	+2.8′	−0.3′
8—9	+2.6′	−1.0′
9—10	+1.4′	+1.1′
10—11	+1.5′	−1.1′
11—12	+1.5′	+0.5′
12—13	+2.1′	−0.5′
13—14	+1.9′	−0.8′
14—15	−1.3′	+0.8′

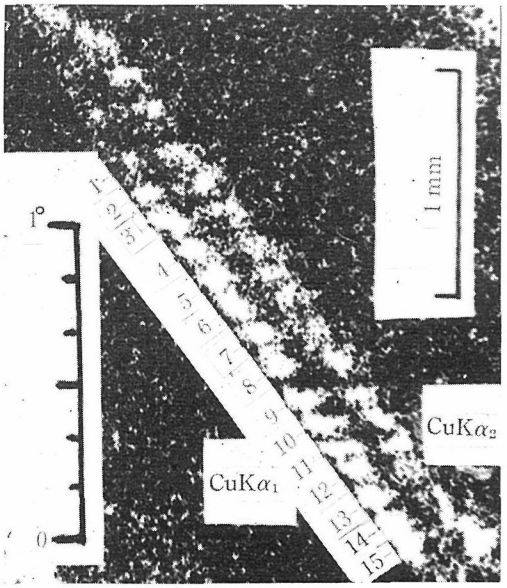

Fig. 5. A (112) reflection of CuKα doublet from a part of the surface of the specimen shown in Fig. 3 (a). $\Delta\theta_h$ and $\Delta\theta_v$ in the table beside the photograph show the misorientation angles between each of the neighbouring reflection spots. The inclination of the reflection lines is attributed to the deviation of the specimen surface from (001).

sepatation or overlap in $\Delta\theta_h$ while the direction of rotation to the right or to the left in $\Delta\theta_v$.

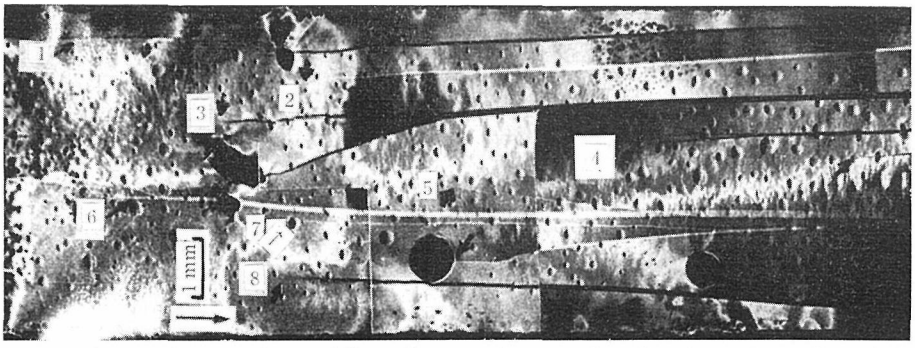

Fig. 6. A set of three pieces of Berg-Barrett photographs taken from the surface of the specimen grown at $R \simeq 1.7 \times 10^{-4}$ cm/sec ($t = 0.015$ cm). The direction of growth is designated with an arrow. The dark and white lines are the separate and overlapped striation subboundaries respectively. The large hollows are the holes penetrating the specimen through both the flat surfaces. The distance from the specimen surface to the plate is larger at the left.

A set of three pieces of Berg-Barrett photographs taken from the surface of the specimen grown at $R \simeq 1.7 \times 10^{-4}$ cm/sec is shown in Fig. 6, where the dark and white lines represent the separate and overlapped subboundaries respectively. No impurity subboundary is observed, but a pair of striation-type subboundaries designated with the numerals 1 and 6 are initially formed keeping a distance of about 2.4 mm ; then after an incubation distance of about 4 mm, another pair of striation subboundaries expressed in the numerals 2 and 3 are further generated between the aforesaid subboundaries keeping a distance of about 0.6 mm ; furthermore, new striation subboundaries expressed in the numerals 5 and 4 are generated after the incubation distances of about 4 mm and 7 mm respectively**. In this case, it should be noticed that the misorientation angles of the newly generated subboundaries gradually increase with growing and finally become constant : this phenomenon is a characteristic feature of the striation subboundary***.

The Berg-Barrett patterns taken from the opposite flat surface to that which is shown in Fig. 6, show the reverse relationship to that in the latter with regard to the misorientation at the mirror-imaged position. So all the subboundaries observed in Fig. 6 have extended to the opposite surface.

Fig. 7 shows a set of five pieces of Berg-Barrett photographs taken from the surface of the specimen grown at $R \simeq 1.5 \times 10^{-4}$ cm/sec. No impurity subboundary is observed as well as in Fig. 6****. A pair of striation subboundaries

** The large hollows observed in the figure are the holes formed in the specimen as mentioned previously, and a new subboundary is always formed after having passed through a hole penetrating the specimen through both the flat surfaces.

*** Since the distance from the specimen surface to the photographic plate is larger at the left, it is clear that the misorientation angle of each subboundary has increased with growth.

**** The impurity subboundaries are observed at the last part of growth. This is attributed

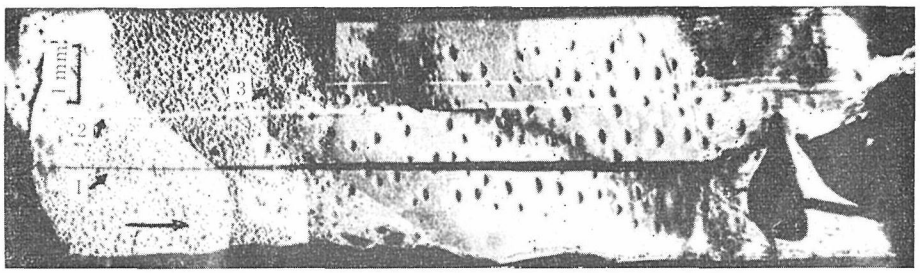

Fig. 7. A set of five pieces of Berg-Barrett photographs taken from the surface of the specimen grown at $R \simeq 1.5 \times 10^{-4}$ cm/sec ($t = 0.015$ cm). Many blowholes are observed and the large hole at the right is a hole penetrating the specimen through both the flat surfaces. The direction of growth is designated with an arrow.

expressed with the numerals 1 and 2, are primarily generated keeping a distance of about 0.9 mm, and then after holding a certain incubation distance, a new striation subboundary expressed with the numeral 3 is generated. The distance from the specimen surface to the photographic plate is larger at the right in this case. So, if the misorientation of the subboundary is constant throughout growth, the overlapped or separate width representing the misorientation of the subboundary, ought to be wider at the right in the figure. Therefore, the misorientation angles of the subboundaries are not always larger at the right than at the left in the figure. So, a further examination was performed under the X-ray irradiation from the reverse direction to that in Fig. 7, but it was confirmed that the misorientation angle of the subboundaries had increased with growth. Furthermore, the subboundary 2 has been genera-

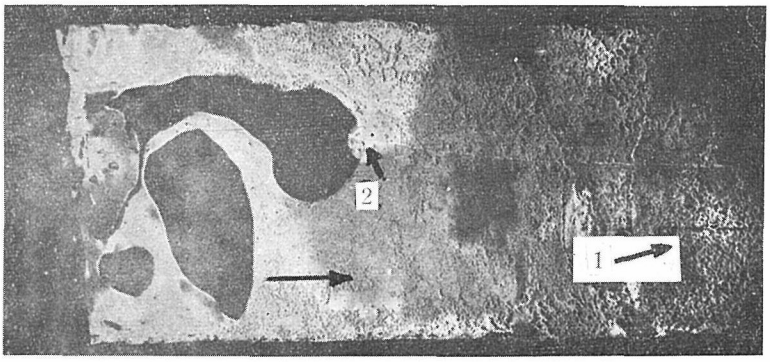

Fig. 8. A Berg-Barrett photograph taken from the first part of the specimen shown in Fig. 7. The direction of growth is designated with an arrow.

ted at a hole in the specimen as shown in Fig. 8, which shows a Berg-Barrett photograph taken from the first part of growth in the specimen shown in Fig. 7. The misorientation angle of this subboundary is almost unchanged until the generation of the subboundary 1, and then increases with a tendency similar to that of the latter. After the generation of the subboundary 3, how-

to the reason that the solute impurities in the specimen are generally accumulated in the last part of solidification. Where the impurity substructure was formed at the last part of the specimen shown in Fig. 6, was not examined.

ever, the misorientation angle of the subboundary 2 does not much increase with growing, whereas that of the subboundary 1 still increases.

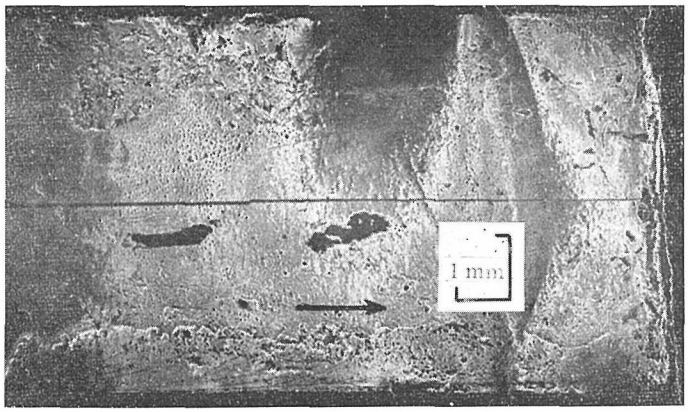

Fig. 9. A Berg-Barrett photograph taken from the last part of the specimen grown at $R \simeq 1.3 \times 10^{-4}$ cm/sec ($t = 0.015$ cm). The arrow designates the direction of growth.

Fig. 9 shows a Berg-Barrett pattern reflected from the last part of growth in the specimen grown at $R \simeq 1.3 \times 10^{-4}$ cm/sec. The distance from the specimen surface to the plate is larger at the left in the figure. Over the whole surface of the specimen, only one separate subboundary is observed. The misorientation angle of this subboundary seems to be constant at $\Delta\theta_v \simeq 1.7'$ and $\Delta\theta_h \simeq 25.9'$ in arc.

iii) Specimens of 0.142 cm in Thickness

Four kinds of specimens grown at $R \simeq 2.4 \times 10^{-2}$, 1.1×10^{-2}, 1.7×10^{-3} and 4.2×10^{-4} cm/sec, were examined by the same X-ray diffraction method as in section (ii) respectively.

On the surface of the specimen grown at $R \simeq 2.4 \times 10^{-2}$ cm/sec, two dendrite crystals whose side arms dévelope only in the directions normal to both the longer edges of the specimen (another direction of easy growth in white tin, $<1\bar{1}0>$) are observed only at both the sides of the specimen.

Concerning the specimen grown at $R \simeq 1.1 \times 10^{-2}$ cm/sec, two kinds of substructures are observed on the whole surface of the specimen, and the widths of almost all striations seem to be similar to those of corrugations and that both kinds of subboundaries always coincide with each other[13)14)].

With regard to the specimen grown at $R \simeq 1.7 \times 10^{-3}$ cm/sec, the impurity substructure is observed over the whole surface of the specimen, while the substructure characterized by the so-called striation is not. Fig. 10 shows a (112) reflection of CuKα doublet from the surface of the spesimen mentioned above. The subboundary whose misorientaion angle is $\Delta\theta_v \simeq -17'$ and $\Delta\theta_h \simeq -32'$ in arc, is observed at the central part, but this subboundary seems to be what has been succeeded from the seed crystal. The misorientation angles of several subboundaries in the figure, are given in the table beside the photograph. Furthermore, this specimen was electro-polished from 0.14 cm to 0.1, 0.07 and 0.05 cm in thickness respectively, and each of the specimen surfaces

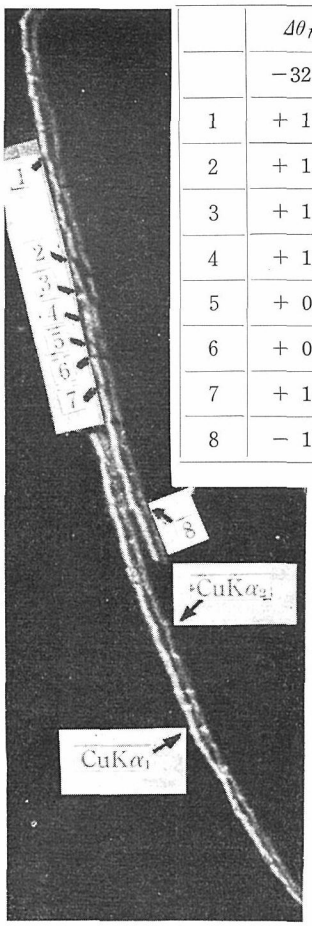

	$\Delta\theta_h$	$\Delta\theta_v$
	−32′	−17′
1	+ 1.5′	+ 2.0′
2	+ 1.0′	− 1.4′
3	+ 1.0′	
4	+ 1.4′	
5	+ 0.8′	
6	+ 0.8′	− 1.0′
7	+ 1.1′	− 1.0′
8	− 1.5′	+ 1.7′

Fig. 10. A (112) reflection of CuKα doublet from the surface of the specimen grown at $R\simeq 1.7\times10^{-3}$ cm/sec ($t=0.142$ cm). $\Delta\theta_h$ and $\Delta\theta_v$ in the table beside the photograph designate the same denotement with those in the table beside the photograph in Fig. 5.

thus electro-polished was examined with X-rays as before. Little remarkable difference from the initial surface of the specimen, however, was found in this specimen.

With regard to the specimen grown at $R\simeq 4.2\times10^{-4}$ cm/sec, the impurity subboundaries which was not straight, were observed over the whole surface of the specimen, and all the striation subboundaries were always found in coincidence with some of the impurity subboundaries as explained in Elbaum's review[1]. Though the inner part of the specimen was also examined as in the specimen grown at $R\simeq 1.7\times10^{-3}$ cm/sec, no essential difference was found.

IV. DISCUSSION

As stated in the foregoing paragraph, many hollows are formed in the specimens, and these undesirable defects will be obstructive to study the generation of substructures in the thin single crystals grown from the melt.

In order to suppress the generation of these defects, it may be effective for molten tin to be charged in vacuum as metioned before.

When one of the flat plates of the glass mould is stripped off from the surface of the specimen, it is desirable for any strain not to be induced. So in this study, the inside of the glass plate was covered with silicon oil. As mentioned before, however, there may be a fear for hollows to be formed. It remains unsolved, therefore, to find out a technique both for getting a fine flat surface and for any strain not to be induced.

The results which were obtained in this study, will be discussed at the stand-point of the mechanism of collapsing vacancy discs. Frank[4] has introduced a following theoretical formula expressing the relationship between the spacing of the striation substructure and the rate of growth:

$$l \simeq 1/R^{1/2} \cdot [D_v \cdot k \cdot T_m^2 / U_f \cdot (dT/dx)]^{1/2}, \qquad (1)^*$$

where l and R denote the spacing in cm and the rate of growth in cm/sec respectively, and D_v is the diffusion coefficient of vacancy, k is Boltzman constant, T_m is the melting temperature, U_f is the energy of formation of a vacancy in the crystal lattice and dT/dx is the temperature gradient in the crystal.

By substituting in the equation (1) the following values are obtained:

$D_v(500°K) \simeq 1.34 \times 10^{-5}$ cm/sec,

$k = 1.35 \times 10^{-16}$ ergs per degree,

$T_m = 505°K$ (melting temperature of tin),

$U_f = U_d/2 \simeq 0.88 \times 10^{-12}$ ergs (U_d: energy of diffusion of a vacancy in the crystal lattice),

$dT/dx = 25°C$/cm,

where the following relations by Schoeck et al.[5] have been assumed:

$D_v(T) \cong D_0 \cdot \exp(-U_m/kT)$ (U_m: energy of migration of a vacancy in the crystal lattice),

$D_0 = 4.35$ cm^2/sec,

$U_m = U_d/2 \simeq 0.88 \times 10^{-12}$ ergs.

The relation of the measured value, l_{exp}, to the evaluated one, l_{calc} will be examined with regard to both the widths of the striations and the corrugations observed in this study. Thus obtained results of both l_{exp} and l_{calc} are tabulated in Table 2: in the column of striation width, the term distance implies the distance between the subboundaries denoted by each numeral; 1-Side, in the last row, implies that the distance from the subboundary 1 to the specimen side is regarded as an assumed one, because of the generation of only one striation subboundary in this specimen; furthermore, the value of $l_{exp} \cdot R^{1/2}$ in the last column should theoretically be 3.16×10^{-3} cm$^{3/2}$/sec$^{1/2}$.

Under the consideration that the impurity subboundary consists of an arrangement of edge-dislocations, the values of both l_{calc} and l_{exp} concerning the corrugation substructure are also given in Table 2, where the unfilled

* For the derivation of this formula, see C. Elbaum's review[1].

Table 2. Experimental results:
l_{calc} and l_{exp} denote the calculated and measured widths of the striations and the corrugations observed in this study respectively, using the equation (1).

R cm/sec	$R^{-1/2}$ sec$^{1/2}$/cm$^{1/2}$	$[D_v \cdot k \cdot T_m^2/U_T \cdot (dT/dx)]^{1/2}$	Striation Width (cm)			$l_{exp} \cdot R^{1/2}$
			l_{calc}	l_{exp}	Distance	
1.7×10^{-4}	76.7	3.16×10^{-3} cm$^{3/2}$/sec$^{1/2}$	0.24	0.24	1-6	3.13×10^{-3}
				0.10	7-8	1.30×10^{-3}
				0.07	4-5	0.91×10^{-3}
				0.06	2-3	0.78×10^{-3}
1.5×10^{-4}	81.7		0.26	0.09	1-2	1.10×10^{-3}
1.3×10^{-4}	87.7		0.28	0.26	1-Side	2.96×10^{-3}
			Corrugation Width (cm)			
○× 1.1×10^{-2}	9.6		0.030	0.006	(Mean Value)	0.63×10^{-3}
○ 2.8×10^{-3}	18.8		0.059	0.010	,,	0.53×10^{-3}
× 1.7×10^{-3}	24.5		0.077	0.013	,,	0.53×10^{-3}
× 4.2×10^{-4}	48.8		0.154	0.013	,,	0.26×10^{-3}
○ 1.5×10^{-4}	81.7		0.258	0.020	,,	0.24×10^{-3}

circle and the cross mark the specimens of 0.015 and 0.142 cm in thickness respectively and the value of l_{exp} is the average one.

The results shown in Table 2 are plotted in Fig. 11 as l_{exp} vs. $1/R^{1/2}$, where the solid line represents the calculated values, l_{calc}, and the filled circle denotes the measured value of the width of striations in the specimens of 0.015 cm in thickness and the unfilled circle and the cross have previously been explained. Furthermore, the dotted line is an experimental line drawn roughly

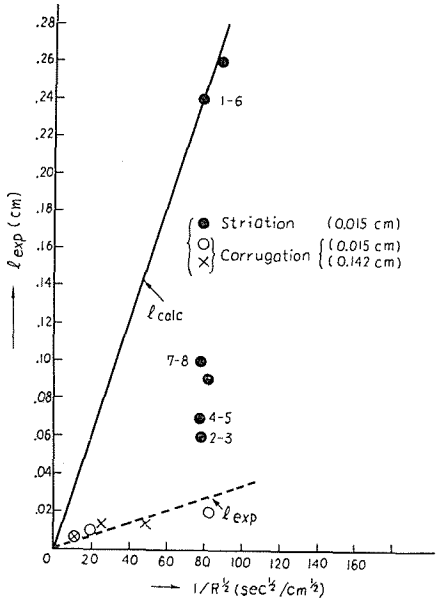

Fig. 11. l_{exp} vs. $1/R^{1/2}$.

concerning the corrugations.

If all the super-saturate vacancies diffuse only towards the direction perpendicular to the flat surface of the specimen, any striation subboundary should not be formed, because all values of l_{calc} are larger than the thickness of the specimen, 0.015 cm. Nevertheless, the striation subboundaries are successively formed. The escape of the super-saturate vacancies from the flat surfaces of the specimen, however, may be disturbed by the oxide film formed on the specimen surfaces. Furthermore, it is supposed that the solid-liquid interface is convex towards the melt, because all the striation subboundaries gradually lean towards both sides of the specimen with growth as observed in Fig. 6. So, the solute atoms rejected into the liquid during freezing may be diffused towards the sides of the specimen. It will be supposed, therefore, that the concentration of solute atoms is richer in both sides of the specimen than in the central part. On the other hand, the concentration of super-saturate vacancies may be larger in the central part of the specimen, because the temperature on a horizontal line drawn in the crystal just behind the solid-liquid interface, may be higher at both sides of the specimen. Consequently, the diffusion of super-saturate vacancies towards both sides of the specimen, may be promoted along the above mentioned concentration gradient of solute atoms.

As seen in Figs. 6 and 11, a pair of new subboundaries expressed in the numerals 2 and 3 are generated between the existing subboundaries 1 and 6, and after an incubation distance, new subboundaries expressed with the numerals 4 and 5 are further formed between the existing subboundaries 3 and 6. Judging from the mechanism of collapsing vacancy discs, the super-saturate vacancies which are newly formed in the crystal, should be diffused out to the existing subboundaries. It is supposed, therefore, that there exist some causes to arrest both the diffusion of super-saturate vacancies and the migration of dislocation rings towards both sides of the specimen. As an extreme case, a correlation of the above mentioned lattice defects with the impurity subboundary may be suggested. Since the slope of the dotted line is much more blunt than that of the solid one in Fig. 11, it is supposed that D_v in the equation (1) is much smaller in the former. Therefore, an effect of the impurities on both the diffusion of vacancies and the migration of dislocation rings, may be supposed. An argument concerning the coincidence of impurity subboundaries with striation ones has already been discussed by one of the authors in the case of nickel single crystals grown from the melt[15].

The super-saturate vacancies existing in the crystal have generally been supposed to aggregate in the close-packed lattice planes—{100}, {110} and {101} in tin—but on what lattice planes the vacancy discs are formed, is unknown yet in this study. All the striation subboundaries formed in the specimens of 0.015 cm in thickness, pierce the specimen through both flat surfaces. Frank's model[4] for the formation of the striation substructure in the square shape, therefore, would not be applicable to our results, but a different type of migration of dislocations generated in the crystal should by supposed. Elbaum[8,10]

has studied by Lang's X-ray method[4] the arrangement of dislocations existing in the high-pure aluminium single crystals grown from the melt. In our study, however, any detailed configuration of dislocations is unknown in the region where no subboundary is observed on the Berg-Barrett patterns. A more detailed examination using an available X-ray method, therefore, will be desierd.

ACKNOWLEDGEMENT

The authors wish to thank Prof. H. Takaki for his encourage ment and useful discussion throughout this study. This work is supported by the research grant of the Ministry of Education.

REFERENCES

(1) e. g., C. Elbaum, Progress in Metal Physics, VIII, 203 (1959); W. C. Winegard, *Metallurgical Rev.*, **6**, 57 (1961).
(2) J. W. Rutter and B. Chalmers, *Canad. J. Phys.*, **31**, 15 (1953).
(3) E. Teghtsoonian and B. Chalmers, *Canad. J. Phys.*, **29**, 370 (1951); **30**, 388 (1952).
(4) F. C., Frank, "Deformation and Flow of Solids", IUTAM Colloquium, Madrid, 73, (1955).
(5) G. Schoeck and W. A. Tiller, *Phil. Mag.*, **5**, 43 (1960).
(6) C. Elbaum, *Phil. Mag.*, **5**, 669 (1960).
(7) K. A. Jackson, *Phil. Mag.*, **7**, 1117 (1962).
(8) C. Elbaum, *J. Appl. Phys.*, **31**, 1413 (1960).
(9) A. R. Lang, *J. Appl. Phys.*, **29**, 597 (1958); Act Cryst., **12**, 249 (1959).
(10) S. Howe and C. Elbaum, *J. Appl. Phys.*, **32**, 742 (1961).
(11) W. von Berg, *Naturwiss.*, **19**, 391 (1931); C. S. Barrett, *Trans. Amer. Inst. Min. Metall. Engrs.*, **161**, 15 (1945).
(12) N. Kato, *Acta Met.*, **5**, 237 (1957); **6**, 647 (1958).
(13) H. Takaki, M. Koyama and H. Fujihira, Bull. Inst. Chem. Res. Kyoto Univ., **33**, 177 (1955).
(14) H. A. Atwater and B. Chalmers, *Canad. J. Phys.*, **35**, 208 (1957).
(15) S. Maeda, Bull. Inst. Chem. Res. Kyoto Univ., **39**, 278 (1961).